jove

# Advances in Nanoscale Infrared Spectroscopy to Explore Multiphase Polymeric Systems

**Rebecca Young**[1,2], **Laurene Tetard**[1,2]

[1] Nanoscience Technology Center, Physics Department, University of Central Florida [2] Physics Department, University of Central Florida

### Corresponding Author

**Laurene Tetard**
**laurene.tetard@ucf.edu**

### Citation

Young, R., Tetard, L. Advances in Nanoscale Infrared Spectroscopy to Explore Multiphase Polymeric Systems. *J. Vis. Exp.* (), e65357, doi:10.3791/65357 (2023).

### Date Published

May 9, 2023

### DOI

10.3791/65357

### URL

jove.com/t/65357

## Abstract

Multiphase polymeric systems encompass local domains with dimensions that can vary from a few tens of nanometers to several micrometers. Their composition is commonly assessed using infrared spectroscopy, which provides an average fingerprint of the various materials contained in the volume probed. However, this approach does not offer any details on the arrangement of the phases in the material. Interfacial regions between two polymeric phases, often in the nanoscale range, are also challenging to access. Photothermal nanoscale infrared spectroscopy monitors the local response of materials excited by infrared light with the sensitive probe of an atomic force microscope (AFM). While the technique is suitable for interrogating small features, such as individual proteins on pristine gold surfaces, the characterization of three-dimensional multicomponent materials is more elusive. This is due to a relatively large volume of material undergoing photothermal expansion, defined by the laser focalization onto the sample and by the thermal properties of the polymeric constituents, compared to the nanoscale region probed by the AFM tip. Using a polystyrene (PS) bead and a polyvinyl alcohol (PVA) film, we evaluate the spatial footprint of photothermal nanoscale infrared spectroscopy for surface analysis as a function of the position of PS in the PVA film. The effect of the feature position on the nanoscale infrared images is investigated, and spectra are acquired. Some perspectives on the future advances in the field of photothermal nanoscale infrared spectroscopy are provided, considering the characterization of complex systems with embedded polymeric structures.

## Introduction

Atomic force microscopy (AFM) has become essential to image and characterize the morphology of a wide variety of samples with nanoscale resolution[1,2,3]. By measuring the deflection of an AFM cantilever resulting from the interaction of the sharp tip with the sample surface, nanoscale functional imaging protocols for local

stiffness measurements and tip-sample adhesion have been developed[4,5]. For soft condensed matter and polymer analysis, AFM measurements exploring the nanomechanical and nanochemical properties of local domains are highly sought after[6,7,8]. Before the emergence of nanoscale infrared (nanoIR) spectroscopy, AFM tips were chemically modified to assess the presence of different domains from the AFM force curve and deduct the nature of the tip-sample interaction. For instance, this approach was used to unveil the transformation of microdomains of poly(tert-butyl acrylate) at the surface of cyclohexane-treated polystyrene-block-poly(tert-butyl acrylate)block copolymer thin films at the sub 50 nm level[9].

The combination of infrared (IR) light with AFM has had a significant impact on the field of polymer science[6]. Conventional IR spectroscopy is a widely used technique for studying the chemical structure of polymeric materials[10,11], but it fails to provide information on individual phases and interphase behavior, as the regions are too small compared to the size of the IR beam used to probe the sample. The problem holds with IR microspectroscopy, as it is restricted by the optical diffraction limit[6]. Such measurements average the contributions of the entire region excited by the IR light; the signals resulting from the presence of nanoscale phases inside the probed region either exhibit complex fingerprints that should be deconvoluted during post-processing or are lost due to a signal level below the detectable level. Hence, it is essential to develop tools capable of nanoscale spatial resolution and high IR sensitivity to explore nanoscale chemical features in complex media.

Schemes to achieve nanoIR spectroscopy have been developed, first using a metallic AFM tip as a nanoantenna[12,13], and more recently exploiting the AFM cantilever's ability to monitor changes in the photothermal expansion incurred during IR illumination of the sample[12,14,15]. The latter uses a pulsed, tunable IR light source tuned to an absorption band of the material probed, which causes the sample to absorb radiation and undergo photothermal expansion. This approach is well-suited for organic and polymeric materials. The pulsed excitation makes the effect detectable by the AFM cantilever in contact with the sample surface in the form of an oscillation. The amplitude of one of the contact resonances of the system observed in the frequency spectrum is then monitored as a function of illumination wavelength, which constitutes the nanoIR absorption spectrum of the material beneath the AFM tip[15]. The spatial resolution of nanoIR imaging and spectroscopy is limited by various effects of the photothermal expansion of the material. It has been evaluated that photothermal nanoIR spectroscopy using contact mode AFM can acquire the vibrational absorption spectra properties of materials with sub 50 nm scale spatial resolution[14], with recent work demonstrating the detection of monomers and dimers of α-synuclein[16,17]. However, quantitative studies of the performance of nanoIR measurements on heterogeneous polymeric materials assembled in various configurations, such as the case of absorbers of finite dimensions embedded in the volume of various polymeric films, remain limited.

This article aims to create a polymeric assembly with an embedded feature of a known dimension to evaluate the sensitivity of photothermal expansion and spatial resolution of nanoIR during surface analysis. The protocol covers the preparation of a polyvinyl alcohol (PVA) polymer thin film on a silicon substrate and the placement of a three-dimensional polystyrene (PS) bead onto or embedded in the PVA film, which constitutes the formation of the model system. NanoIR imaging and spectroscopy measurements are described in

the context of evaluating the signals generated by the same PS bead positioned on or beneath the PVA film. The influence of the bead position on the nanoIR signals is evaluated. Methods to assess the spatial footprint of the bead in the nanoIR map are discussed, and the effects of several parameters are considered.

## Protocol

### 1. Making polyvinyl alcohol (PVA) solution

1. Measure water and PVA polymer pellets (see **Table of Materials**) to create a 10 mL solution at a 20% PVA to water ratio by weight.
2. Heat the water in the glassware over a hot plate set to 100 °C.
3. Place the PVA polymer pellets into the heated water. Insert a magnetic stir bar.
4. Reduce the heat to 80 °C and stir until the PVA fully dissolves.
5. Cover the top of the glassware to prevent contamination.
6. Once fully dissolved, place the 20% PVA solution into an appropriate storage container for storage at room temperature.

### 2. Preparing PVA-coated silicon (Si) wafers

1. Cut a silicon (Si) wafer (see **Table of Materials**) into ~10 x 10 $mm^2$ squares.
2. Clean the Si substrate using isopropyl alcohol and let it dry.
3. Place the clean Si wafer on the chuck of the spin coater (see **Table of Materials**).
   1. Drop cast approximately 10 µL of PVA solution onto the center of the Si wafer. Try to avoid bubble formation.
   2. Coat the Si substrate with a uniform PVA film by spin coating for 30 s at 1,500 rotations per minute (rpm).
      NOTE: The specified volume of liquid and spin coating parameters create a uniform layer of PVA across the surface of the wafer with sufficient thickness to prevent rapid drying between the spin coating and placing the PS beads onto the PVA surface in the next step.
4. Remove the sample from the spin coater and place it into a clean sample container to prevent contamination before transferring the PS beads.

### 3. Placing the PS beads onto the PVA-coated surface

1. Clean a Si substrate using isopropyl alcohol and let it dry.
2. Using a pipette, place 1 µL of PS beads suspended in water onto the center of the substrate.
3. Let the water evaporate by placing the sample in a storage compartment containing bentonite clay desiccant.
   NOTE: This step preserves the sample by reducing exposure to humidity.
4. Place the PVA-coated substrate (step 2.4) and the substrate with the dried PS beads (step 3.3) under an optical microscope. Depending on their size, a single bead will be visible using simple binoculars or will require higher optical magnification.
5. Gently loosen the beads using ultrafine tweezers (see **Table of Materials**). Use a fine hair paintbrush to collect a few loose beads and lightly tap the hairs of the

paintbrush over the freshly PVA-coated wafer. Multiple sweeps should allow the beads to accumulate within the hairs of the brush. Tap the top of the paintbrush hairs to disturb the PS bead powder to release beads onto the tacky PVA surface.

NOTE: It is important that the paintbrush is of high quality and clean to avoid releasing fibers and contaminants onto the PVA film's surface. Moving quickly during this step is essential so that the PVA does not completely dry.

6. Repeat this step until it is confirmed by optical microscopy inspection that individual PS beads adhere to the PVA surface.

7. Store the sample in a clean container. Allow the sample to dry fully.

NOTE: The sample should be allowed to cool and dry completely before further analysis attempts are performed. AFM height measurements or surface profiler measurements can assess the thickness of successive PVA films.

## 4. Loading the sample for AFM characterization

NOTE: The protocol described is based on standard operating procedures of a nanoIR2 (see **Table of Materials**) platform, but should be adapted according to the AFM model used for the measurement.

1. Mount the PVA and PS bead sample onto the AFM stage using a metallic AFM disk and adhesive tabs, so that the sample is firmly attached to the sample holder.

2. Mount a nanoIR probe (e.g., FORTGG) onto the AFM probe holder.

NOTE: The AFM cantilever is 225 µm long, 27 µm wide, and 2.7 µm thick, with a tip radius of less than 10 nm. The cantilever is coated with 45 nm thick gold film on both sides to limit its response to the top-side IR illumination of the sample (see **Table of Materials**). For nanoIR spectroscopy measurements, preferably use a cantilever that has been stored in a polydimethylsiloxane-free environment prior to use.

3. Align the read-out laser at the free end of the cantilever beam by turning the laser alignment knobs (x and y adjustments of the laser position and vertical adjustment of the detector position).

    1. Maximize the SUM signal of the detector.

    2. Adjust the position of the detector by turning the deflection knob so that the laser is aligned with the center of the position-sensitive detector of the AFM read-out system, corresponding to a vertical deflection signal of ~0 V.

4. Click on the **Load** icon in the AFM "Probe" control panel.

    1. Follow the prompts within the wizard screen. Use the **focus arrows** to determine the focal plane of the nanoIR cantilever. Use the XY-displacement controls to position the cantilever in the center of the screen (aligned with the white cross).

    2. Next, click on the **focus arrows** to find the focal plane of the surface of the sample.

    3. Use the optical view of the system and the XY-displacement controls to position the cantilever tip above the bead of interest and click on **Next**.

    4. On the engage screen, set the "standoff" to **50 µm** and click on **Approach Only**.

5. Initiate the **Engage** procedure to approach the tip for imaging.

## 5. Creating topographical and nanoIR images of the multipolymer sample

1. Acquire topography images in standard "Contact Mode". Once the position of the cantilever with respect to the PS bead is set, initiate the approach by clicking on the **engage** icon in the AFM "Probe" control panel. An engage setpoint of a deflection differential of 0.2 V is used for the entire study here, corresponding to a force of ~100 nN.

    1. In the AFM "Scan" control panel, set the **scan rate** to 0.8 Hz, **scan size** (height and width), and the **number of points per line and number of lines per image** to use for imaging (512 x 512 was used here). Click on Scan to acquire the topography image.

        NOTE: Calibration of the cantilever[18] is done by determining the deflection sensitivity (in nm/V) from the slope of the deflection-distance curve obtained with the cantilever interacting with a sapphire substrate (**Supplementary Figure 1A**). The cantilever stiffness is determined from thermal tuning[19] (**Supplementary Figure 1B**). The resonance of the cantilever is fitted using a Lorentzian function. The cantilever stiffness (in Nm/m) is determined using the equipartition theorem $k = \frac{K_B T}{P}$, where $K_B$ is the Boltzmann constant, T is the temperature (T = 295K), and P is the area of the power spectrum of the thermal fluctuations of the cantilever determined by integrating the Lorentzian fit of the thermal tuning data[20].

2. For nanoIR measurements, position the AFM tip on the feature of interest identified from the topography image.

1. Select the **tuning fork** icon in the nanoIR control panel to determine the contact resonance frequencies of the cantilever. Set an illumination wavenumber that will excite photothermal expansion in the material. Set a range of laser pulse frequency to sweep and set the duty cycle of the nanoIR laser. Select **Acquire** within the "Laser Pulse Tune Window".

2. Select the second contact resonance of the tip-sample system for nanoIR measurements by positioning the marker bar (green vertical line) at the peak of the second contact resonance.

    NOTE: The selection of the contact resonance mode can vary depending on the type of cantilever and sample.

3. Click on **Optimize** to align the center of the IR laser focal region with the position of the cantilever tip. Alignment is done at a selected IR illumination wavenumber, corresponding to an absorption band of the material probed. The cantilever is positioned at the center of the laser footprint (**Supplementary Figure 2**).

    NOTE: Alignment can vary for different wavenumbers depending on the laser model.

4. Acquire a background of the IR laser illumination. This consists of measuring the output of the IR quantum cascade laser (QCL) in the wavelength range of emission at the pulse frequency selected (**Supplementary Figure 3**). This is important for background correction of the nanoIR spectra.

5. Acquire the nanoIR spectrum by selecting the wavenumber range (here, **Start** and **Stop** are set to 1,530 $cm^{-1}$ and 1,800 $cm^{-1}$, respectively), the **step**

**size** (2 $cm^{-1}$), and the **number of averages** used for the measurement. Perform background correction of the spectra displayed by dividing the photothermal amplitude measured by the attenuated background, which consists of multiplying the background collected in step 5.2.4 by the percentage of power selected for the measurement.

3. For nanoIR imaging, select the **region of interest** for imaging.
    1. Enable **phase-locked loop (PLL) auto-tune** in the "Laser Pulse Tune Window" (accessed by the **Tuning fork** icon).
    2. Adjust the minimum and maximum frequency to create a sweep range centered at the second resonance mode in the general control panel.
    3. Zero the phase by clicking on **zero** in the PLL control panel and then click on **OK** in the "Laser Pulse Tune window".
    4. Select **IR Imaging Enabled** by putting a checkmark in the box within the nanoIR control panel.
    5. In the "Imaging View" control panel, choose **Height** (Imaging View 1), **Amplitude 2** (Imaging View 2), and **Phase2** (Imaging View 3) to acquire the topographical and chemical images of the sample. Set the acquisition direction to **Trace** (or **Retrace**). A line fit **Line** is often required to observe the topography image of the sample being acquired. Capture fit should be set to **None**.

        NOTE: Scanning preferences, such as scan direction captured or color palette used, can be adjusted as needed.
    6. In the AFM "Scan" control panel, select the **Scan** icon.
    7. To save the image, select the **Now** or **End of frame** icon in the "Capture" control panel.
4. To export the data, right-click on the image or spectrum file names within the data lists. Select **Export** and choose the format of the file to export. Save the file in the desired computer folder location.

## Representative Results

PS ($(C_8H_8)_n$) beads were deposited on a clean Si substrate (**Figure 1A**) and on PVA ($(CH_2CHOH)_n$) (**Figure 1B,C**). Due to the poor adhesion of the bead on Si, nanoIR imaging in contact mode could not be acquired for this sample. Instead, using the optical view of the sample on nanoIR, the gold-coated AFM probe was engaged on top of the PS bead in contact mode, with an estimated force of about 100 nN (**Figure 2A**). The pulsed IR laser was set to excite the sample at 1,730 $cm^{-1}$, since both PS and PVA are expected to absorb at this wavenumber. The pulse frequency of the laser was swept to determine the contact resonance of the cantilever for the nanoIR spectrum measurement. When pulsed at the contact resonance frequency, the cantilever response was monitored to determine the amplitude of the oscillation (**Figure 2B**). Next, the nanoIR spectra were constructed by monitoring the amplitude of the contact resonance as a function of the illumination wavenumber, from 1,530 to 1,800 $cm^{-1}$ in steps of 2 $cm^{-1}$ (**Figure 2C**). In this range (**Figure 3A**, inset), the spectrum revealed the presence of two IR bands centered at 1,600 $cm^{-1}$ and 1,730 $cm^{-1}$, corresponding to the predominant stretch mode of the phenyl moiety and a subset of the ring stretching in PS, respectively[21]. Comparing the nanoIR spectrum with the far-field Fourier transform infrared (FTIR) spectrum of PS confirmed the presence of the aromatic mode at 1,600 $cm^{-1}$ (**Figure 3A**). However, it was noted that the relative amplitude $I_{1600}/I_{1730}$ was

significantly different in the FTIR and nanoIR spectra, with respective values of 2.9 and 0.9. This was attributed to the mechanism of detection of nanoIR spectroscopy, which monitors the photothermal expansion of the polymer instead of its absorbance, as in the FTIR spectroscopy. In the case of PS, this corresponded to a higher photothermal expansion when exciting the aromatic sub-bands at 1,730 $cm^{-1}$. The nanoIR spectrum of PVA exhibited better agreement with the FTIR spectrum with a predominant absorption band centered at ~1,730 $cm^{-1}$ (**Figure 3B**). While this band was not expected in pure PVA, which does not contain a C=O group, prior work suggests that the presence of the band can be attributed to carbonyl functional groups due to residual acetate used in the preparation of PVA (rate as ~80%-90% hydrolyzed)[22]. For the purpose of this study, the presence of a band at 1,730 $cm^{-1}$ was suitable to assess the effect of simultaneous absorption of PS and PVA.

The nanoIR spectra were used to select the illumination wavenumbers for chemical imaging of the PS bead deposited at the surface of PVA (**Figure 4A-C**) and of the PS bead coated with PVA (**Figure 4D-F**). The PLL contact resonance frequency tracking capability of the system was used to ensure that the amplitude measurement at each pixel corresponded to the maximum amplitude of the contact resonance peak[15] (**Figure 2C**). The contact resonance of the cantilever was measured when the cantilever tip was in contact with PVA and PS to determine a suitable range of the PLL frequency tracking.

NanoIR images were first acquired at 1,600 $cm^{-1}$, which corresponds to the case where PS is the predominant absorber of the system (**Figure 4A**i; **D**i)). Although a 5 µm PS bead was imaged in both cases, the amplitude of the photothermal expansion recorded at this wavelength was different when the tip was directly in contact with the PS bead and when the tip was in contact with the thin PVA coating on top of the PS bead. The increase in photothermal expansion detected above the PS bead was significantly smaller when the bead was covered with the layer of PVA, estimated to be ~1.8 µm thick using a surface profiler (**Supplementary Figure 4**). At the laser power used (1.47%, which corresponds to ~3.4 mW at 1,600 $cm^{-1}$ and ~3.8 mW at 1,730 $cm^{-1}$) (**Supplementary Table 1**), a region ~13 µm in diameter exhibited a slight increase in amplitude ~2 nm above the signal recorded on the pure non-absorbing PVA layer away from the PS bead. The spatial footprint of the amplitude increase was much broader than when the PS bead was on top of the PVA film (**Figure 4A**), where the photothermal expansion signal was asymmetrical but remained contained within a region ~6 µm wide in the fast scan direction and ~8 µm long in the slow scan direction of the image. The amplitude readings in this region reached up to 12.1 nm above the photothermal expansion of the pure PVA layer. When illuminating the sample at 1,730 $cm^{-1}$, PS and PVA both exhibited a higher amplitude of photothermal expansion than at 1,600 $cm^{-1}$. In the case of the exposed PS bead (**Figure 4C**i), the photothermal expansion was highest on top of the bead, reaching values up to 26.5 nm. The high photothermal response extended several micrometers beyond the footprint observed in **Figure 4A**i. The PVA also expanded due to the excitation, but at a lower amplitude, namely ~7.6 nm recorded away from the PS bead. It was noted that the response was consistently strongest on the left side of the PS bead. For the embedded bead (**Figure 4F**), the signal was more symmetrical, but the amplitude of the photothermal expansion above the PS bead was only ~2.3 nm higher than that of the PVA. For this, a consistent photothermal amplitude of ~13.6 nm was recorded within the 10-13 µm footprint of the region affected by PS heating,

determined from mapping the surface with the AFM probe. In the case of measurements carried out at 1,620 $cm^{-1}$, no signal was detected, which is consistent with the absence of a notable IR absorption band for PS and PVA in this region of spectrum.

Next, the nanoIR spectra collected on top of a PS bead covered was compared with PVA (**Figure 5A**). The PS signal at 1,600 $cm^{-1}$ was significantly lower than in the case of the uncovered bead. Despite the low contribution of the band, further analysis of the signals confirmed that increasing the laser power led to a higher ratio $I_{1600}/I_{1730}$ (**Figure 5B,C**). The results suggested that a higher laser power corresponds to larger penetration depth, as depicted in **Figure 5B**. In turn, this affects the nanoIR image collected under a different laser power. At a higher power of ~20 mW, the photothermal amplitude of the material consistently exhibited a lower amplitude than at lower laser powers. Further, the noise level in the spectra increased, suggesting some instabilities in the material, likely due to the increase in temperature in the polymer.

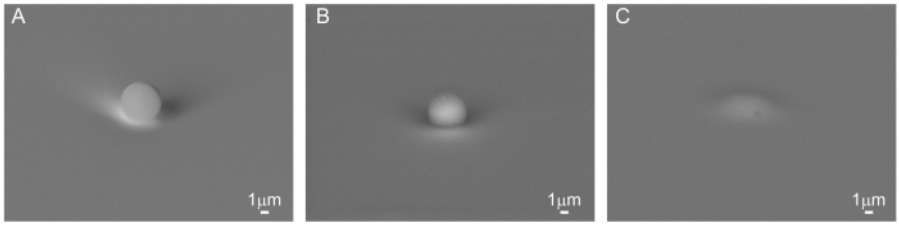


**Figure 1: Deposition of PS beads.** Scanning electron microscopy (SEM) image of the 5 µm PS bead (**A**) on top of a pristine silicon substrate, (**B**) on top of a PVA film, and (**C**) covered with PVA. Scale bar = 1 µm. Please click here to view a larger version of this figure.

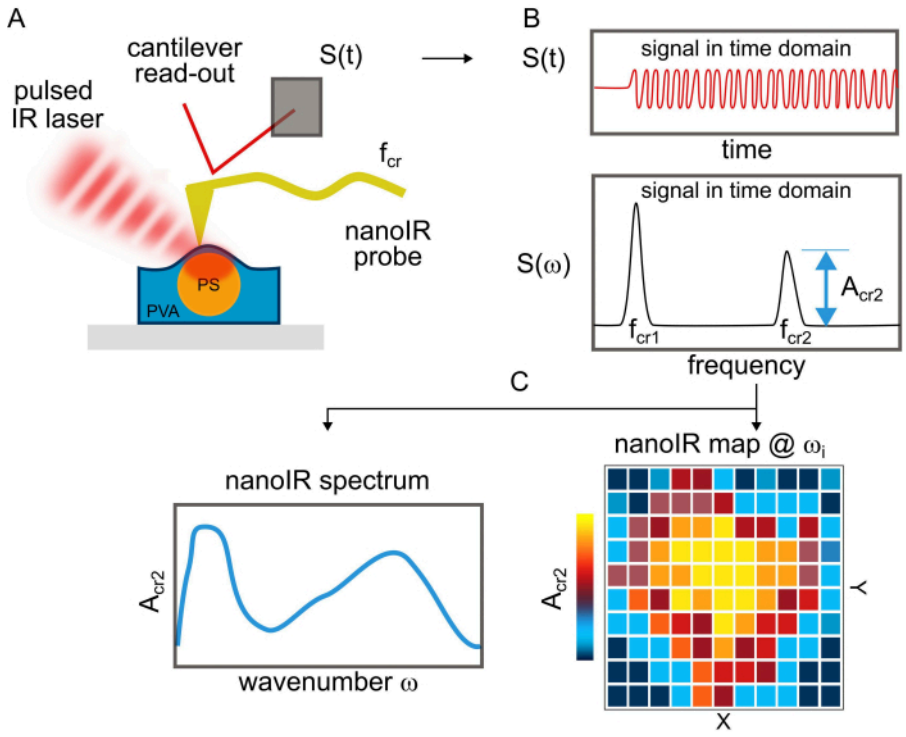


**Figure 2: Schematics illustrating the principle of nanoIR imaging and spectroscopy.** (**A**) The IR pulsed laser is aligned and focused onto the point of contact of the metallic AFM cantilever tip with the sample. The cantilever measures the photothermal response of the material resulting from IR absorption. The gold layer on both sides is used to reduce the photothermal and acoustic contribution of the cantilever during the measurement, which would interfere with the nanoIR measurement of the sample. (**B**) Signal of the position-sensitive detector monitoring the deflection of the cantilever in the time domain [S(t)] and frequency domain [S(w)]. The contact resonance modes of the cantilever are identified by lock-in amplifier measurements. The second contact resonance is used for PLL tracking during imaging. The amplitude of the contact resonance mode $A_{cr2}$ is measured. (**C**) NanoIR spectrum obtained by monitoring the change in amplitude $A_{cr2}$ as a function of illumination wavenumber. The NanoIR image was obtained by monitoring the change in amplitude $A_{cr2}$ as a function of the position of the tip on the sample. Please click here to view a larger version of this figure.

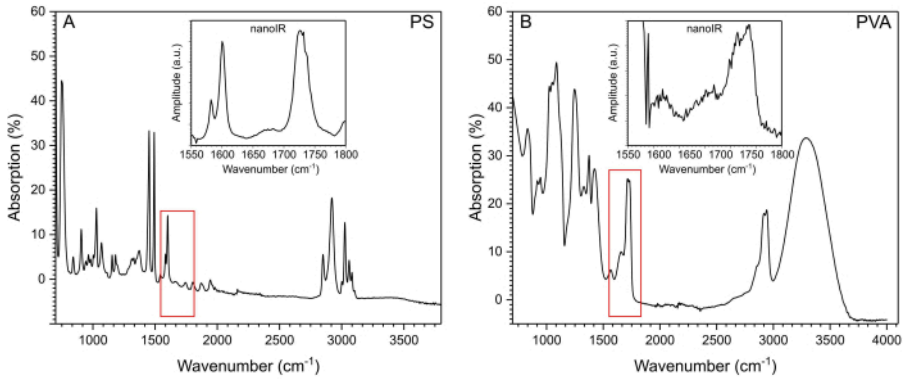


**Figure 3: IR spectra of PS and PVA.** (**A**) FTIR spectrum of PS. The red box indicates the range of the spectrum studied with nanoIR spectroscopy. The corresponding nanoIR PS spectrum is provided in the inset. (**B**) FTIR spectrum of PVA. The red box indicates the range of the spectrum studied with nanoIR spectroscopy. The corresponding nanoIR PVA spectrum is provided in the inset. Please click here to view a larger version of this figure.

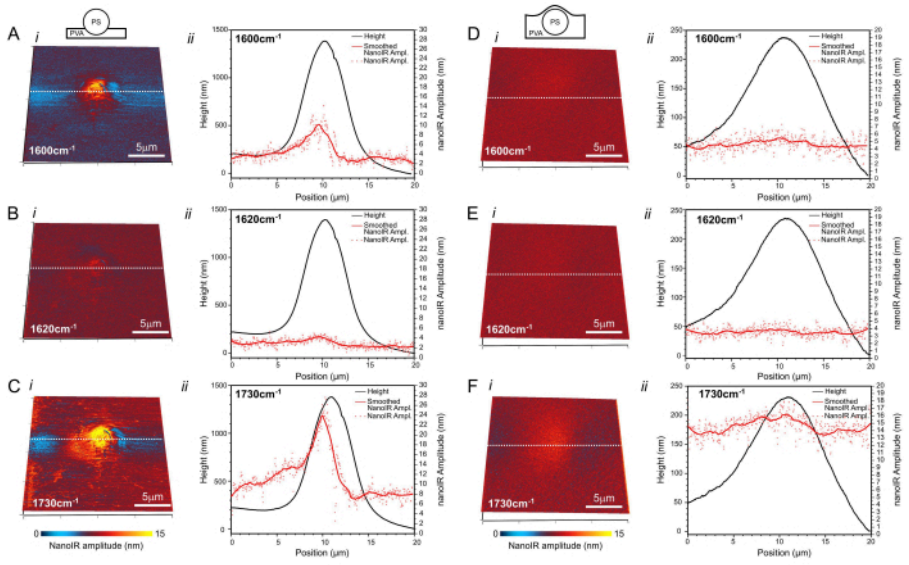


**Figure 4: NanoIR imaging.** The PS bead (**A-C**) deposited on the surface of PVA and (**D-F**) embedded in PVA as depicted in the insets. NanoIR maps acquired at (**A**i,**D**i) 1,600 $cm^{-1}$, (**B**i,**E**i) 1,620 $cm^{-1}$, and (**C**i,**F**i) 1,730 $cm^{-1}$ are overlayed on the 3D topography map. Corresponding topography and nanoIR profiles extracted along the white dashed line are presented in the respective graphs (ii). Scale bar = 5 µm. Please click here to view a larger version of this figure.

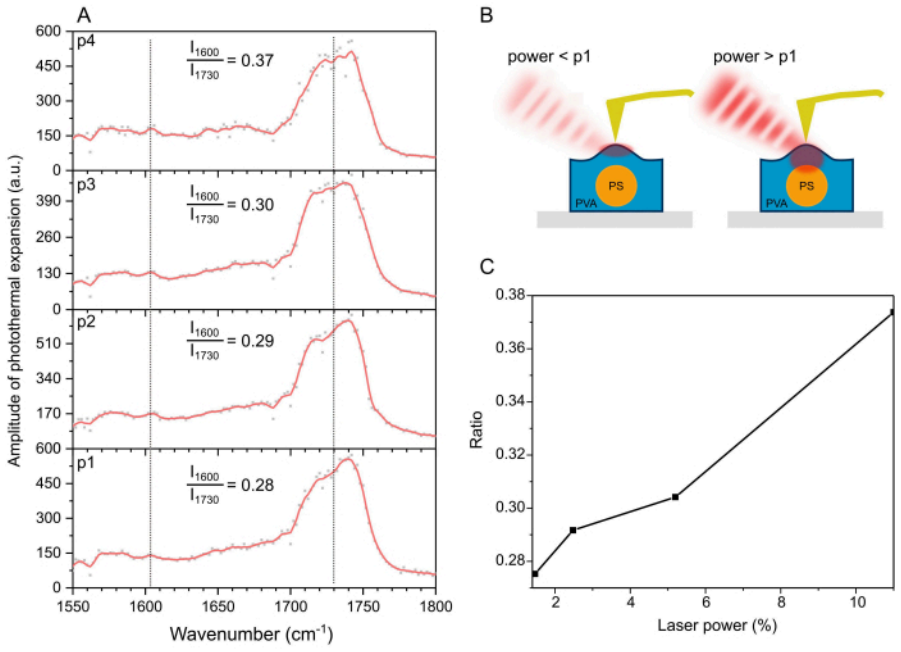


**Figure 5: NanoIR spectrum collected by the AFM tip in contact with the PS bead coated with PVA.** (**A**) NanoIR spectra collected at p1 = 1.47%, p2 = 2.48%, p3 = 5.20%, and p4 = 11% of the laser power. Laser power varies as a function of wavelength, which is corrected for by attenuated background correction for each case. (**B**) Schematics illustrating the effect of laser power on the strength of the signals collected. (**C**) Ratio $I_{1600}/I_{1730}$ as a function of laser power. Please click here to view a larger version of this figure.

**Supplementary Figure 1: Calibration of the nanoIR cantilever.** (**A**) Deflection-distance curve obtained on a sapphire substrate. The slope of the retract curve provides the deflection sensitivity of the cantilever used to calculate the spring constant. (**B**) Cantilever resonance frequency determined by thermal tuning used to calculate the spring constant. Please click here to download this File.

**Supplementary Figure 2: IR laser footprint.** The oscillation amplitude of the cantilever in contact with the sample surface is recorded as a function of the position of the IR laser. The IR laser alignment is varied using a moving mirror. The position of the mirror is set to align the center of the focal volume (red region) with the position of the cantilever (center of the white cross). Please click here to download this File.

**Supplementary Figure 3: Laser output power (in mW) as a function of wavenumber.** The output power of the QCL laser is determined using a standard IR detector from 1,530 $cm^{-1}$ to 1,800 $cm^{-1}$ in steps of 2 $cm^{-1}$ at the pulse frequency corresponding to the setting used for the nanoIR measurements. Please click here to download this File.

**Supplementary Figure 4: PVA thickness measurements obtained by laser confocal surface profilometry.** Please click here to download this File.

**Supplementary Table 1: The laser power in milliwatts for each wavenumber.** Please click here to download this File.

## Discussion

AFM combined with nanoIR spectroscopy can provide nanoscale chemical information using a cantilever in contact mode and a pulsed tunable IR light source. Model systems, such as embedding an absorber with finite dimensions in the volume of a polymeric material, are important to improve the understanding of image formation mechanisms and to determine the performance of the tool. In the case of the PS/PVA configuration presented here, optimization was carried out to obtain a stable PS bead positioned above or below the surface of the PVA film. It was found that depositing the PS beads immediately after removing the coated wafer from the spin coater resulted in better adhesion. The viscosity of the PVA layer can affect the positioning of the bead with respect to the PVA film surface. Heating the sample for approximately 15 min at ~200 °C allowed for deeper implantation of the beads.

Thanks to the size of the PS beads (5 µm here), rapid alignment of the cantilever tip with the center of the bead is possible using the optical microscope built-in with the nanoIR system. While PS beads and microbubbles in the PVA can hardly be differentiated optically, nanoIR analysis can confirm the composition of the sample. While the contribution of the IR band at 1,600 $cm^{-1}$ can be weak when the PS bead is covered with another polymer, as noted in **Figure 5**, high laser power can increase the contribution of PS at 1,600 $cm^{-1}$ in the nanoIR fingerprint collected directly above it, with the cantilever in contact with the PVA overlay. It is expected that PS beads with smaller diameters will be more difficult to locate with optical microscopy and will contribute a lower signal to the nanoIR spectrum. In such a case, AFM imaging and nanoIR measurements of the PS beads before deposition of the top-coat layer of PVA should be considered, together with marking the sample to ensure that the location of the embedded PS beads is known. Despite these foreseen challenges, this approach to prepare model systems has the benefit of being cheap and readily available. The profile of the topography of the bead could be used to estimate the bead position, though the so-called tip effect should be taken into account to assess the diameter of the feature imaged.

Regarding data acquisition and analysis, the data produced with nanoIR in this study reveal several unexpected instabilities of the tip-sample interaction when using a softer nanoIR cantilever and when increasing the laser power. NanoIR images collected with a softer cantilever ($k < 0.4$ N/m) are consistently unstable near the PS bead excited by the IR light, despite a stable topography image. The nanoIR spectra of PS and PVA recorded in this study are in good agreement with the commonly reported FTIR spectra of the corresponding bulk polymers[21,22]. The two distinct bands of absorption at 1,600 $cm^{-1}$ (PS only) and 1,730 $cm^{-1}$ (PS and PVA) provide a way to compare the effect of exciting the single bead absorber beneath the surface. The nanoIR images presented in **Figure 4** indicate that the signal in the vicinity of the bead is strong when the PS bead is exposed but decreases significantly when a PVA thin film covers the bead. However, the results indicate that a bead more than 1 µm below the surface can be detected in the nanoIR map, both when exciting the system at 1,600 $cm^{-1}$ and at 1,730 $cm^{-1}$. The amplitude detected by the cantilever increases by ~2 nm directly above the bead in the map in both cases. Although low in amplitude, the footprint of this expansion is about 13 µm wide for the 1,600 $cm^{-1}$ excitation, which is much larger than the diameter of the bead, confirming that heat diffuses from the PS absorber to the PVA. This Joule expansion can affect

the spatial resolution of nanoIR on heterogeneous materials, with a stronger effect expected if the absorber is closer to the surface. The larger response of the sample at 1,730 $cm^{-1}$ is consistent with the nanoIR spectra presented in **Figure 5**, showing that the contribution of the band at 1,600 $cm^{-1}$ is much weaker than at 1,730 $cm^{-1}$.

The current approach presents some limitations. Positioning the beads below the surface of PVA while limiting the topographical bump on the surface of the model system remains unattainable. In fact, it may require such a thick coating that the bead could become undetectable from the point of view of nanoIR spectroscopy. The depth of the bead is both difficult to control and to characterize, which would make it difficult to provide sufficient information for modeling for an accurate representation of the model system. A more complete picture of the effect of the subsurface absorber size and depth on the nanoIR signal measured at the surface would require varying the dimensions and positions of the bead with greater precision. In addition, it is likely that in a real complex system, several subsurface absorbers with different sizes, positions, and compositions would interfere with the measurements, which is not described in this model.

Nonetheless, the measurements confirm that there is much to learn from signal generation on multi-polymeric samples for nanoIR characterization. Further optimization of the sample preparation protocol should be undertaken to controllably vary the depth at which the PS bead is embedded to allow a more comprehensive analysis of how the photothermal expansion at the surface of PVA is impacted by the subsurface absorber. The combination of polymers used for the measurements can also be varied to determine the role of thermal conductivity, thermal expansion, and mechanical properties on the performance of the nanoIR measurements for heterogeneous materials. This constitutes a promising approach to better understand the behavior of the sample for nanoIR spectroscopy and imaging, and is expected to facilitate the quantification of penetration depth, spatial resolution, and sensitivity of the tool further. This is particularly important given the emergence of new modes of imaging, such as multi-frequency nanoIR[15,23], for which the nature of the information and the effect of actuation parameters on the performance of the tools remain poorly understood. To deepen the understanding of the data collected, it will be critical to combine the experimental approach with Multiphysics modeling[24]. Considering embedded features of different sizes and varying their position beneath the surface will be critical to develop a more comprehensive model. In turn, this will advance the field of nanoIR spectroscopy toward applications of real-life heterogeneous and three-dimensional materials.

## Disclosures

The authors have nothing to disclose.

## Acknowledgments

This work was supported by the National Science Foundation (NSF CHE-1847830).

## References

1. Dufrêne, Y. F., Viljoen, A., Mignolet, J., Mathelié-Guinlet, M. AFM in cellular and molecular microbiology. *Cellular Microbiology.* **23** (7), e13324 (2021).
2. Sharma, A., Rout, C. S. Probe-based techniques for 2D layered materials. in *Advanced Analytical Techniques for Characterization of 2D Materials.* AIP Publishing. Melville, New York. 5-1-5-14 (2022).

3. Zhong, J., Yan, J. Seeing is believing: atomic force microscopy imaging for nanomaterial research. *RSC Advances.* **6** (2), 1103-1121 (2016).
4. Olubowale, O. H. et al. "May the force be with you!" Force-volume mapping with atomic force microscopy. *ACS Omega.* **6** (40), 25860-25875 (2021).
5. Dokukin, M. E., Sokolov, I. Quantitative mapping of the elastic modulus of soft materials with HarmoniX and PeakForce QNM AFM modes. *Langmuir.* **28** (46), 16060-16071 (2012).
6. Nguyen-Tri, P. et al. Recent applications of advanced atomic force microscopy in polymer science: a review. *Polymers.* **12** (5), 1142 (2020).
7. Vitry, P. et al. Mode-synthesizing atomic force microscopy for 3D reconstruction of embedded low-density dielectric nanostructures. *Nano Research.* **8** (7), 2199-2205 (2015).
8. Coste, R., Pernes, M., Tetard, L., Molinari, M., Chabbert, B. Effect of the interplay of composition and environmental humidity on the nanomechanical properties of hemp fibers. *ACS Sustainable Chemistry & Engineering.* **8** (16), 6381-6390 (2020).
9. Schönherr, H., Feng, C. L., Tomczak, N., Vancso, G. J. Compositional mapping of polymer surfaces by chemical force microscopy down to the nanometer scale: reactions in block copolymer microdomains. In *Macromolecular Symposia.* Weinheim. **230** (1), 149-157 (2005).
10. Holland-Moritz, K., Siesler, H. W. Infrared spectroscopy of polymers. *Applied Spectroscopy Reviews.* **11** (1), 1-55 (1976).
11. Bhargava, R., Wang, S. Q., Koenig, J. L. FTIR microscpectrscopy of polymeric systems. in *Liquid Chromatography/FTIR Microspectroscopy/Microwave Assisted Synthesis.* Springer Berlin Heidelberg Berlin. Heidelberg. 137-191 (2003).
12. Rao, V. J. et al. AFM-IR and IR-SNOM for the characterization of small molecule organic semiconductors. *The Journal of Physical Chemistry C.* **124** (9), 5331-5344 (2020).
13. Wang, H., Wang, L., Xu, X. G. Scattering-type scanning near-field optical microscopy with low-repetition-rate pulsed light source through phase-domain sampling. *Nature Communications.* **7** (1), 13212 (2016).
14. Dazzi, A., Prater, C. B. AFM-IR: Technology and applications in nanoscale infrared spectroscopy and chemical imaging. *Chemical Reviews.* **117** (7), 5146-5173 (2017).
15. Mathurin, J. et al. Photothermal AFM-IR spectroscopy and imaging: Status, challenges, and trends. *Journal of Applied Physics.* **131** (1), 010901 (2022).
16. Miller, A. et al. Enhanced surface nanoanalytics of transient biomolecular processes. *Science Advances.* **9** (2), eabq3151 (2023).
17. Emin, D. et al. Small soluble α-synuclein aggregates are the toxic species in Parkinson's disease. *Nature Communications.* **13** (1), 5512 (2022).
18. Jardine, K., Dove, A., Tetard, L. AFM force measurements to explore grain contacts with relevance for planetary materials. *The Planetary Science Journal.* **3** (12), 273 (2022).
19. Sader, J. E., Chon, J. W. M., Mulvaney, P. Calibration of rectangular atomic force microscope cantilevers. *Review of Scientific Instruments.* **70** (10), 3967-3969 (1999).

20. Higgins, M. J. et al. Noninvasive determination of optical lever sensitivity in atomic force microscopy. *Review of Scientific Instruments.* **77** (1), 013701 (2006).

21. Smith, B. The infrared spectra of polymers III: hydrocarbon polymers. *Spectroscopy.* **36** (11), 22-25 (2021).

22. Korbag, I., Mohamed Saleh, S. Studies on the formation of intermolecular interactions and structural characterization of polyvinyl alcohol/lignin film. *International Journal of Environmental Studies.* **73** (2), 226-235 (2016).

23. Tetard, L., Passian, A., Farahi, R. H., Thundat, T., Davison, B. H. Opto-nanomechanical spectroscopic material characterization. *Nature Nanotechnology.* **10** (10), 870-877 (2015).

24. Bai, Y., Yin, J., Cheng, J.-X. Bond-selective imaging by optically sensing the mid-infrared photothermal effect. *Science Advances.* **7** (20), eabg1559 (2021).